THE JOURNAL OF PHYSICAL CHEMISTRY A

Article

Cite This: J. Phys. Chem. A 2018, 122, 420−430

pubs.acs.org/JPCA

An *ab Initio* Exploration of the Bergman Cyclization

Adam R. Luxon,[†] Natalie Orms,[‡] René Kanters,[†] Anna I. Krylov,[‡] and Carol A. Parish*[,†]

[†]Department of Chemistry, University of Richmond, Richmond, Virginia 23173, United States

[‡]Department of Chemistry, University of Southern California, Los Angeles, California 90089, United States

Supporting Information

ABSTRACT: The Bergman cyclization is an important reaction in which an enediyne cyclizes to produce a highly reactive diradical species, *p*-benzyne. Enediyne motifs are found in natural antitumor antibiotic compounds, such as calicheamicin and dynemicin. Understanding the energetics of cyclization is required to better control the initiation of the cyclization, which induces cell death. We computed the singlet and triplet potential energy surfaces for the Bergman cyclization of (*Z*)-hex-3-ene-1,5-diyne using the CCSD and EOM-SF-CCSD methods. The triplet enediyne and transition state were found to have C_2 symmetry, which contrasts with the singlet reactant and transition state that possess C_{2v} symmetry. We analyzed the frontier orbitals of both cyclization pathways to explain the large energetic barrier of the triplet cyclization. Reaction energies were calculated using CCSD(T)/cc-pVTZ single-point calculations on structures optimized with CCSD/cc-pVDZ. The singlet reaction was found to be slightly endothermic (ΔH_{rxn} = 13.76 kcal/mol) and the triplet reaction was found to be highly exothermic (ΔH_{rxn} = −33.29 kcal/mol). The adiabatic singlet−triplet gap of *p*-benzyne, computed with EOM-SF-CCSD/cc-pVTZ, was found to be 3.56 kcal/mol, indicating a singlet ground state.

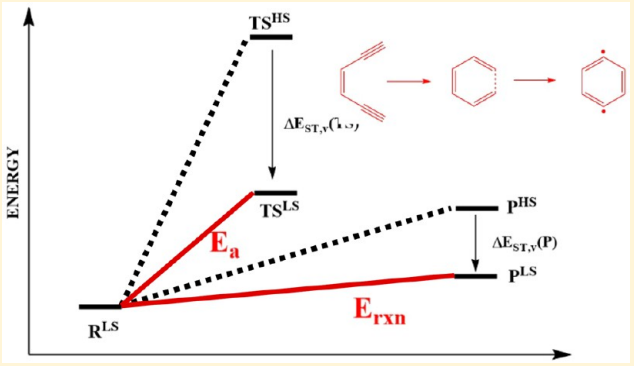

INTRODUCTION

The enediyne (*Z*)-hex-3-ene-1,5-diyne (**R**) undergoes Bergman cyclization via a transition state (**TS**) to form *p*-benzyne (**P**), a highly reactive diradical species that readily abstracts hydrogens (Scheme 1).[1] This fundamental reaction can be triggered either thermally, to proceed along the singlet potential energy surface, or photochemically, to proceed along the triplet surface.[2−7] The Bergman cyclization is of interest because enediynes may be precursors to aromatic species in interstellar medium[8] and because natural enediynes are potent antitumor antibiotics.[9−11]

Scheme 1. Bergman Cyclization of (*Z*)-Hex-3-ene-1,5-diyne

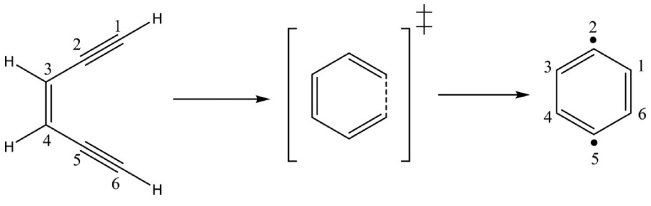

Since the discovery of natural enediynes, the reaction described in Scheme 1 has been the subject of several theoretical studies.[12−21] The structure of the singlet reactant (^{1}**R**) has been determined experimentally.[22] The ground state structures of ^{1}**R**, ^{1}**TS**, and ^{1}**P** have been studied with numerous theoretical methods such as density functional theory (DFT), complete active space self-consistent field (CASSCF), multiconfigurational second-order perturbation (CASPT2), coupled-cluster with singles and doubles and perturbative triples (CCSD(T)), and many-body perturbation theory (MBPT).[12−20] The triplet surface has been explored with CASSCF and CASPT2.[15,19] The electronic structure and energetics of **P** have been investigated extensively, with an emphasis on excited states and singlet−triplet energy gaps. The adiabatic singlet−triplet gap ($\Delta E_{ST,a} = E_T - E_S$) was experimentally determined to be 3.8 ± 0.4 kcal/mol.[23] Theoretical results vary widely on the basis of the methods used.[15,19,24−26]

The Bergman cyclization is a fundamentally important reaction; however, the stationary points on the singlet and triplet surfaces have not yet been characterized using a uniform computational approach capable of capturing the essential features underlying the electronic structure. This is a challenging reaction to study because of the multiconfigurational nature of ^{1}**P**, and the possible multiconfigurational nature of ^{1}**TS**. Due to its diradical character, **P** features extensive electronic degeneracies.[24,27,28] As a result, the ground state singlet possesses a multiconfigurational wave function, making it theoretically interesting and challenging to characterize.[19,24,27,29−31] Methodologies capable of capturing this

Received: October 25, 2017
Revised: December 11, 2017
Published: December 11, 2017

DOI: 10.1021/acs.jpca.7b10576
J. Phys. Chem. A 2018, 122, 420−430

multiconfigurational character must be applied to account for the multiple electronic configurations. For quantitative accuracy, which is very important for reproducing energy differences between nearly degenerate states, dynamical correlation should also be included. Here we employ the spin-flip (SF) approach,[32] which accurately describes singlet and triplet diradical wave functions without the need to select an active space or important configurations. Importantly, the SF method provides a balanced description of dynamical and nondynamical correlation.

The SF approach developed by Krylov was originally designed for characterizing bond breaking, but its ability to describe diradicals was soon realized.[32,33] SF methods can accurately describe low-spin multiconfigurational states by treating them as spin-flipping excitations from a single-configuration high-spin reference state.[32,33] The SF ansatz describes the multiconfigurational singlet and triplet target states in the following way[33]

$$^{3,1}\Psi_{M_s=0} = R_{M_s=-1}\,{}^{3}\Psi_{M_s=+1} \quad (1)$$

where $^{3}\Psi_{M_s=+1}$ is the $\alpha\alpha$ high-spin reference wave function, $R_{M_s=-1}$ is the spin flipping excitation operator, and $^{3,1}\Psi_{M_s=0}$ are the target singlet and triplet wave functions. Because all $M_s = 0$ determinants can be obtained from a single spin-flip excitation out of the high-spin reference, all $M_s = 0$ configurations are treated in a balanced fashion using a single reference formalism (Figure 1).

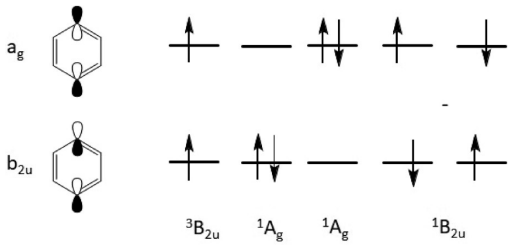

Figure 1. Various ways to distribute two electrons in two nearly degenerate σ orbitals for **P**. All four $M_s = 0$ determinants, pictured on the right, can be obtained from the single $M_s = 1$ Slater determinant with just one spin-flipping excitation.

By using a reference wave function that is accurately described by a single configuration, SF methods do not involve a multireference formalism and do not depend on a user-defined active space. SF methods are size extensive and perform well for excited states, diradicals, triradicals, and bond breaking, with an accuracy approaching 1 kcal/mol.[27,32−37] The description of the target states[27,38] can be systematically improved by increasing the level of electron correlation treatment.[39] In this study, we employ the SF model based on the equation-of-motion coupled-cluster with single and double excitations (EOM-SF-CCSD).[40−42] Though EOM-SF-CCSD has been used to describe the structures and electronic states of the benzyne diradicals, this is the first SF characterization of all stationary points along the lowest lying singlet and triplet surfaces of the Bergman cyclization.

To gain insight into underlying electronic structure, we use density-based wave function analysis tools,[43−45] which enable mapping the correlated many-body wave functions into a simple 2-electrons-in-2-orbitals picture shown in Figure 1. These tools allow us to quantify the degree of radical character associated with the reactant, transition state, and product along the singlet and triplet pathways. By using natural orbitals of the correlated one-particle density, this approach allows one to visualize the true frontier molecular orbitals. This analysis is independent of the choice of molecular orbitals used in the calculation (i.e., Hartree−Fock, Kohn−Sham, etc.) and includes correlation effects. The occupations of the natural orbitals can be used to define the number of effectively unpaired electrons.[46−48]

COMPUTATIONAL DETAILS

We carried out all calculations using the Q-Chem electronic structure package.[49] We used the *libwfa* module[43,44] of Q-Chem to compute and visualize natural orbitals and the Head-Gordon index. Orbital visualization was performed using IQmol[50] and Jmol.[51]

Optimizations and Frequency Calculations. We performed all optimizations and frequency calculations with the cc-pVDZ and cc-pVTZ basis sets. The results reported here are computed using the structures optimized with cc-pVTZ, unless otherwise noted. We optimized ^{1}**R** with CCSD using a restricted Hartree−Fock (RHF) reference. Because the diradical nature of ^{1}**TS** was unknown, we optimized the structure using EOM-SF-CCSD with an unrestricted Hartree−Fock (UHF) high-spin $^{3}B_1$ (C_{2v} point group) reference. We also employed EOM-SF-CCSD to optimize the structure of ^{1}**P**. The SF optimization of ^{1}**P** used the high-spin $^{3}B_{2u}$ (D_{2h} point group) UHF reference.

We optimized the structures of ^{3}**R**, ^{3}**TS**, and ^{3}**P** using UHF-CCSD. Frequency calculations at the same level of theory as the geometry optimization were carried out to confirm all geometries and to determine zero-point energy (ZPE) contributions.

Energy Calculations. To calculate accurate activation barriers (E_a) and reaction energies (E_{rxn}), the reactant energetics must be obtained with the same method as the energetics of the transition state and product. However, this is challenging because ^{1}**R** is a well-behaved closed-shell species whereas ^{1}**TS** and ^{1}**P** are possibly open-shell multiconfigurational species, making it difficult to find a method that describes all three structures with a similar accuracy. This problem is not present in the triplet pathway because ^{3}**R**, ^{3}**TS**, and ^{3}**P** are all well represented by a single high-spin determinant and can therefore be accurately described by the single-reference CCSD method.

To overcome the methodological challenges the singlet pathway presents, we followed a protocol similar to that of Cristian et al.:[52] we used the energetics of the high-spin (HS) pathway and the vertical singlet−triplet gaps ($\Delta E_{ST,v}$) to calculate the E_a and E_{rxn} of the low-spin (LS) pathway. Figure 2 illustrates this approach. We note that this strategy is akin to exploiting isodesmic reactions for obtaining accurate thermochemical values.[53−55] Such approaches, which are designed to provide balanced description of all species involved in the reaction, ensure efficient error cancellation and deliver the best quality results for a given level of theory.[56,57]

Using singlet structures that were optimized in the manner described above, we performed single-point calculations using CCSD(T) with a restricted open-shell HF (ROHF) reference and the cc-pVTZ basis set. For ^{1}**R**, the ground state singlet total energy was calculated (R^{LS}). For ^{1}**TS** and ^{1}**P**, the total energy for the lowest lying triplet was calculated (TS^{HS}, P^{HS}). All three states (R^{LS}, TS^{HS}, and P^{HS}) are single-configurational

DOI: 10.1021/acs.jpca.7b10576
J. Phys. Chem. A 2018, 122, 420−430

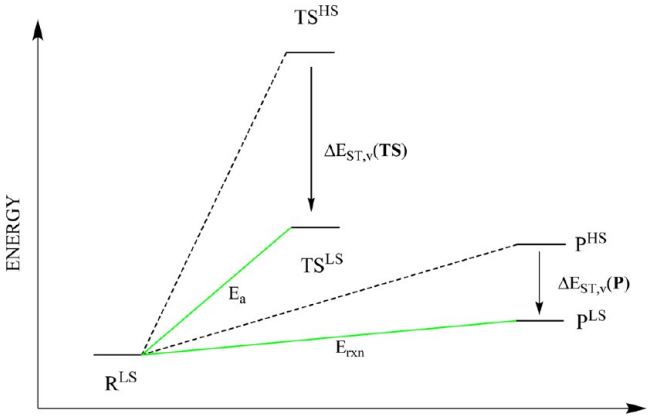

Figure 2. Determination of E_a and E_{rxn} for the singlet reaction pathway. All geometries correspond to the ground-state singlet wave function. Single-point calculations of triplet states at the singlet geometries (TS^{HS}, P^{HS}) were performed using CCSD(T)/ROHF/cc-pVTZ. Singlet−triplet vertical gaps were calculated using EOM-SF-CCSD/ROHF/cc-pVTZ.

and are well described by the CCSD(T) method, which we used to calculate the high-spin reaction barrier ($E_a^{HS} = TS^{HS} - R^{LS}$) and reaction energy ($E_{rxn}^{HS} = P^{HS} - R^{LS}$). We carried out EOM-SF-CCSD/ROHF/cc-pVTZ calculations to obtain accurate vertical ΔE_{ST} for ^{1}**TS** and ^{1}**P**. To obtain E_a^{LS} and E_{rxn}^{LS}, we subtracted the $\Delta E_{ST,v}$ for ^{1}**TS** and ^{1}**P** from E_a^{HS} and E_{rxn}^{HS}, respectively:

$$E_a^{LS} = E_a^{HS} - \Delta E_{ST}(\mathbf{TS})$$
$$E_{rxn}^{LS} = E_{rxn}^{HS} - \Delta E_{ST}(\mathbf{P}) \quad (2)$$

Note that the structures of the high-spin states are not optimized; eq 2 uses vertical singlet−triplet energy gaps computed at the singlet structures.

SF calculations with an unrestricted reference may be affected by spin-contamination.[36,58] To mitigate spin-contamination, we used ROHF-based references when calculating the energetics. For geometry optimization, we used a UHF reference because analytic gradients are not yet available for ROHF EOM-SF-CCSD. A detailed comparison of the energetics computed with restricted (RHF and ROHF) and unrestricted (UHF) references is presented below and in the Supporting Information.

We also carried out single-point calculations at the CCSD/UHF/cc-pVTZ optimized triplet stationary points for the triplet pathway using the CCSD(T)/ROHF/cc-pVTZ and EOM-SF-CCSD/ROHF/cc-pVTZ levels of theory. We calculated adiabatic gaps as the difference in total energy between the SF target state corresponding to the $M_s = 0$ component of the triplet at the triplet-optimized structure and the lowest lying singlet SF target state at the singlet-optimized structure. We calculated vertical gaps at each of the six optimized structures by taking the difference between the $M_s = 0$ component of the triplet and the lowest lying singlet.

To compute and visualize natural orbitals and the number of effectively unpaired electrons, we used the *libwfa* module[43,44] of Q-Chem. Natural orbitals are eigenstates of the one-particle density matrix and their eigenvalues can be interpreted as the occupation numbers, n_i. Using the spin-average occupation numbers, $\bar{n}_i$, several ways to compute an effective number of unpaired electrons have been proposed.[46−48] In this work, we made use of the $n_{u,nl}$ index, proposed by Head-Gordon[47] as an extension of work by Yamaguchi et al.:[46]

$$n_{u,nl} = \sum \bar{n}_i^2 (2 - \bar{n}_i)^2$$

Natural orbitals along the singlet pathway correspond to the lowest lying EOM-SF-CCSD/cc-pVDZ singlet states obtained from the high-spin triplet reference using singlet geometries. Natural orbitals along the triplet pathway were obtained from the high-spin triplet at the CCSD/cc-pVDZ level of theory using triplet geometries. In all figures, we only show α orbitals, as the shapes of paired α and β natural orbitals are the same.

We report $n_{u,nl}$ and natural occupations of the frontier orbitals. Because the current implementations of the SF methods are not spin-adapted, the SF states show some (usually small) spin-contamination even if ROHF references are employed. Consequently, α and β frontier orbitals (and the respective occupations) are slightly different. Below we report spin-average natural occupation, $\bar{n}$, as well as the difference between the α and β natural occupations:

$$\bar{n} = |n_\alpha + n_\beta|$$
$$\Delta n = |n_\alpha - n_\beta|$$

The latter quantity provides an additional measure of spin-contamination.

RESULTS AND DISCUSSION

Below we discuss the geometries and electronic structure of each species along the singlet and triplet pathway, followed by a discussion of the energetics of the two pathways.

Singlet Pathway (S_0). ^{1}**R**, ^{1}**TS**, and ^{1}**P** have C_{2v}, C_{2v}, and D_{2h} point group symmetry, respectively (Figure 3). The ^{1}**R** structure reported in this study (calculated at the CCSD/cc-pVTZ level) agrees well with previous studies; our value of the critical C_1-C_6 distance is 0.057 Å larger than the experimentally derived value of 4.321 Å.[22] The geometry of ^{1}**TS** is very product-like, which is in agreement with previous theoretical results.[15,19,21] The geometry of ^{1}**TS** is relatively insensitive to the level of theory; for example, geometries computed by SF-DFT with B3LYP and B50505LYP with the 6-31G* basis set are in good agreement with the SF-CCSD structure. The geometry of ^{1}**P** is a distorted benzene structure with the bonds between the two carbons attached to a hydrogen, r_{34} and r_{16}, longer than the C−C bonds containing a radical center. This distortion is reported in other theoretical studies as well.[15−17,19,24,29] Table S1 in the Supporting Information compares our SF-CCSD geometries with the results of previous computational studies.

^{1}**R** is a well-behaved closed-shell species. The highest occupied molecular orbital (HOMO) and the lowest unoccupied molecular orbital (LUMO) correspond to the C_3-C_4 $\pi(2b_2)$ and $\pi^*(2a_2)$ orbitals, respectively. This suggests that a HOMO to LUMO excitation would effectively break the C_3-C_4 π bond. The large vertical singlet−triplet gap (ΔE_{ST}) of 130.9 kcal/mol (*vide infra*) in ^{1}**R** supports this idea.

The electronic structure of ^{1}TS is dominated by a closed-shell configuration with a weight of 79%. The next configuration contributes less than 5% (Table 1). The number of effectively unpaired electrons for this state is 0.09 (Table 2). Thus, both wave function analysis and Head-Gordon indices indicate that the transition state is electronically more reactant-like than product-like.[21] The HOMO and LUMO are the

DOI: 10.1021/acs.jpca.7b10576
J. Phys. Chem. A 2018, 122, 420−430

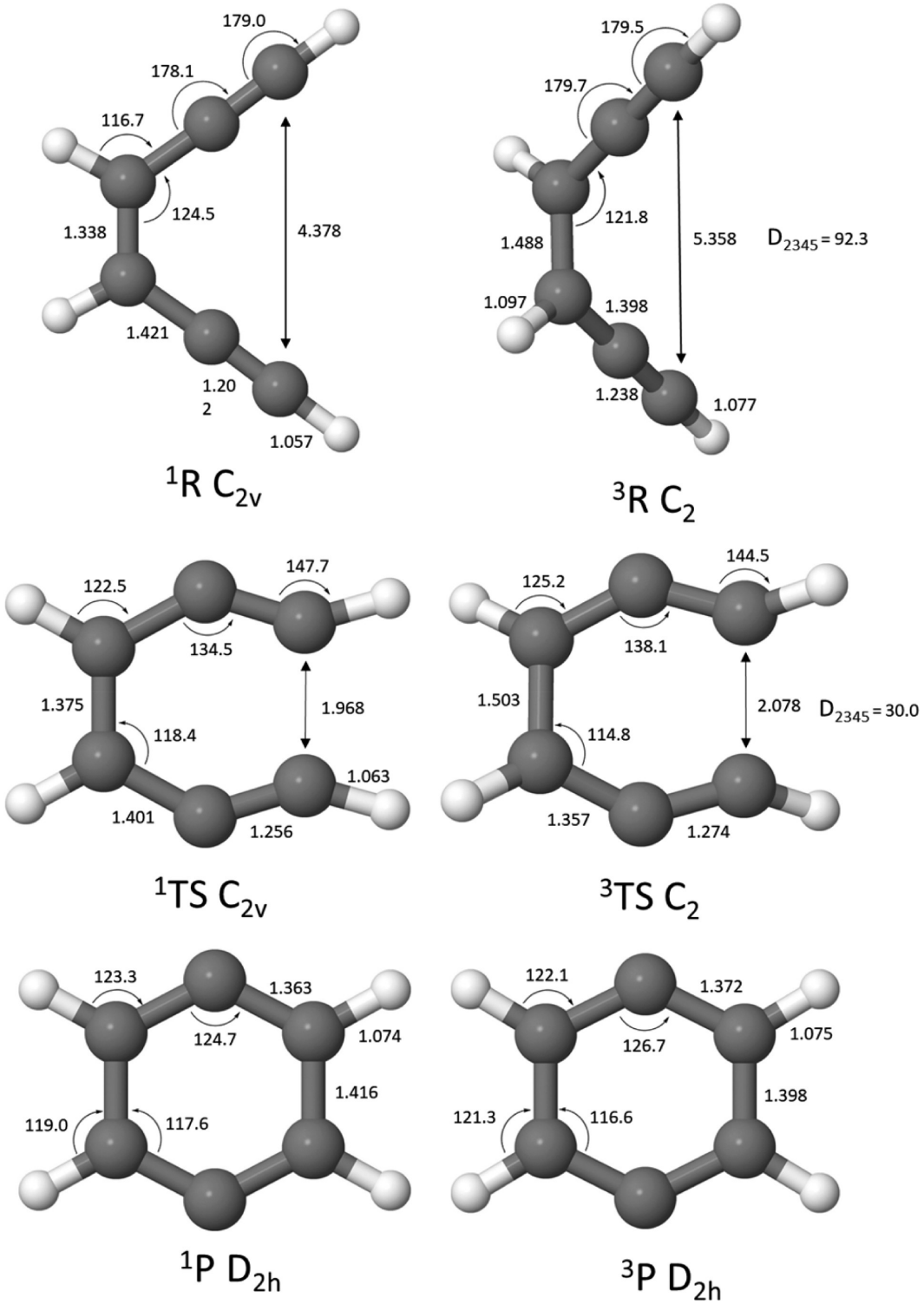

Figure 3. Stationary points along the singlet and triplet pathways. ^{1}R optimized with CCSD/cc-pVTZ. ^{1}TS and ^{1}P optimized with EOM-SF-CCSD/cc-pVTZ. ^{3}R, ^{3}TS, and ^{3}P optimized with CCSD/cc-pVTZ. Images generated with Jmol. Distances are reported in angstroms and angles are reported in degrees.

antisymmetric ($8b_1$) and symmetric combination ($10a_1$) of the C_2 and C_5 radical lobes, respectively, which suggests that there is coupling through the C_3-C_4 σ bond.[59,60]

The ground state of **P** is a singlet that exhibits a multiconfigurational wave function with two leading configurations (Table 1) and $n_{u,nl}$ = 0.28. The dominant configuration has the asymmetric combination of radical orbitals ($5b_{2u}$) doubly occupied and lower in energy than the symmetric combination ($6a_g$), a result of through bond coupling.[59,60]

Triplet Pathway (T_1). Equilibrium structures of ^{3}**R**, ^{3}**TS**, and ^{3}**P** have C_2, C_2, and D_{2h} point group symmetry, respectively. The "arms" of ^{3}**R** distort out of plane 92.3° and the C_3-C_4 bond length is 1.488 Å, indicating that the double

DOI: 10.1021/acs.jpca.7b10576
J. Phys. Chem. A 2018, 122, 420−430

Table 1. Leading Electronic Configurations of Singlet and Triplet States at the Respective Optimized Structures

state	orbital occupancy[a]
^{1}**R**	90% [Core]^{30}, $1b_2^2$, $1a_2^2$, $9a_1^2$, $8b_1^2$, $2b_2^2$, $2a_2^0$, $12a_1^0$
^{3}**R**	78% [Core]^{30}, $9a^2$, $8b^2$, $9b^2$, $10a^2$, $11a^1$, $10b^1$,$14a^0$
^{1}**TS**	79% [Core]^{30}, $1b_2^2$, $9a_1^2$, $1a_2^2$, $2b_2^2$, $8b_1^2$, $10a_1^0$, $2a_2^0$
^{3}**TS**	80% [Core]^{30}, $9a^2$, $8b^2$, $10a^2$, $9b^2$, $10b^1$, $11a^1$, $12a^0$
^{1}**P**	53% [Core]^{30}, $5a_g^2$ $1b_{1u}^2$, $1b_{3g}^2$, $1b_{2g}^2$, $5b_{2u}^2$, $6a_g^0$, + 24% [Core]^{30}, $5a_g^2$ $1b_{1u}^2$, $1b_{3g}^2$, $1b_{2g}^0$, $5b_{2u}^0$, $6a_g^2$
^{3}**P**	77% [Core]^{30}, $5a_g^2$ $1b_{1u}^2$, $1b_{3g}^2$, $1b_{2g}^2$, $5b_{2u}^1$, $6a_g^1$

[a][Core]^{30} denotes the first 15 doubly occupied lower energy molecular orbitals.

Table 2. Wavefunction Properties of the Reactant, Transition State, and Product in the Singlet and Triplet Pathways of the Bergman Cyclization

state	$n_{u,nl}$	$\langle S^2 \rangle$
^{1}**R**	0.10	0.05
^{3}**R**	2.21	2.00
^{1}**TS**	0.09	0.03
^{3}**TS**	2.25	2.00
^{1}**P**	0.28	0.01
^{3}**P**	2.19	2.02

bond present in ^{1}**R** is weakened in ^{3}**R**. Similarly, ^{3}**TS** is distorted out of plane by 30° and the C_3-C_4 bond is elongated to 1.503 Å. The geometry of ^{3}**TS** is relatively insensitive to methodological treatment; geometries computed by B3LYP and B50505LYP with the 6-31G* basis set are in good agreement with the CCSD structure. The structure of ^{3}**P** is very similar to that of ^{1}**P**, with the exception that there is more delocalization in the triplet, as indicated by smaller differences between r_{12} and r_{16}. Table S2 compares the CCSD geometries reported here with the results of previous computational studies.

The distortion of ^{3}**R** can be explained by analyzing the molecular orbitals (MO) of ^{1}**R** and ^{3}**R**. As mentioned above, the HOMO and LUMO of ^{1}**R** are the C_3-C_4 π and π^* orbitals. A HOMO to LUMO excitation would result in a triplet state with a single electron in both the π and π^* orbitals, reducing the bond order to 1. Without the π bond to hold the arms of ^{3}**R** in plane, they are free to rearrange to minimize electronic repulsion. The resulting singly occupied molecular orbitals (SOMO), 11a and 10b, are the in-phase and out-of-phase combinations, respectively, of the two *p*-orbitals on C_3 and C_4. In ^{1}**R**, the same C_3 and C_4 *p*-orbitals combine to make the π and π^* orbitals, $2b_2$ and $2a_2$. In ^{3}R, the nonplanarity of the enediyne causes the C_3 and C_4 *p*-orbitals to adopt a nearly perpendicular orientation, which reduces their interaction and causes the SOMOs (10b, 11a) of ^{3}**R** to be nearly degenerate (Figure 4). Visualization of the unpaired spin density and frontier natural orbitals shows that in ^{3}**R** the unpaired electrons are localized to C_3 and C_4 *p*-type orbitals (Figure 5, 6, and 7). This arrangement allows some bonding interaction, which is why in ^{3}**R** the C_3-C_4 bond length is shorter (1.488 Å) than a standard C−C single bond.

This process is reversed as the triplet reaction pathway proceeds and the molecule becomes more planar. The SOMOs of ^{3}**TS** are the analogous orbitals of the ^{3}**R** SOMOs. The ^{3}**TS** SOMOs are a combination of *p*-orbitals on C_3-C_4 and *p*-orbitals on C_1 and C_6. ^{3}**TS** is planar enough that the in-phase

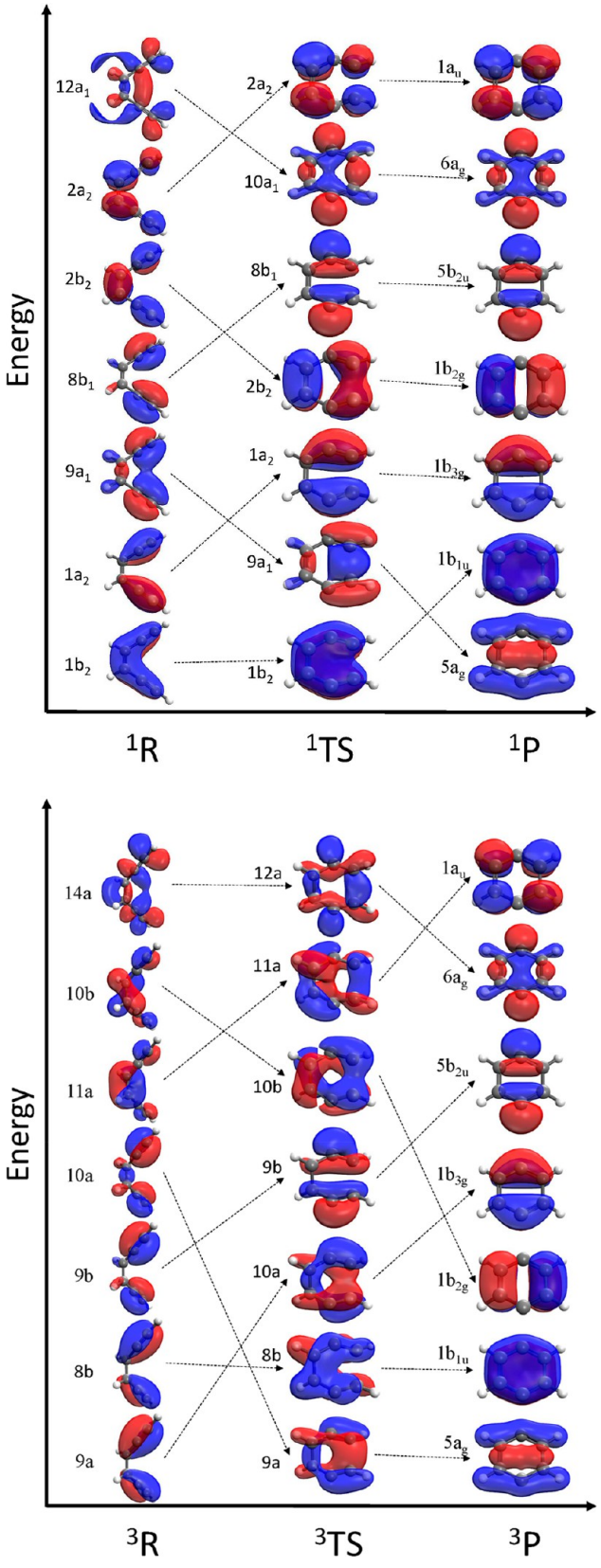

Figure 4. Transformation of frontier molecular orbitals along the singlet (top) and triplet (bottom) reaction coordinate. Orbitals were obtained using the HF/cc-pvTZ triplet reference state at the CCSD/UHF/cc-pVDZ optimized structures.

DOI: 10.1021/acs.jpca.7b10576
J. Phys. Chem. A 2018, 122, 420−430

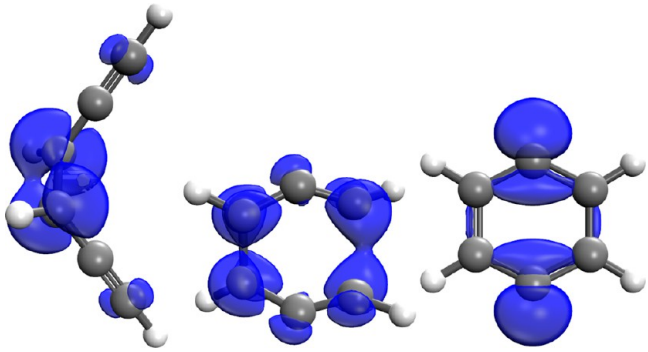

Figure 5. Unpaired spin densities for triplet optimized structures. From left to right: ^{3}**R**, ^{3}**TS**, ^{3}**P**. Isovalue of 0.075. IQmol used for visualization.

and out-of-phase combinations of the C_3-C_4 p-orbitals form π and π^* orbitals, each occupied by a single electron (Figure 5, ^{3}**TS**, orbitals 11a and 10b). Consequentially, there is only a single bond between C_3-C_4, as evidenced by the bond length. Our C_3-C_4 bond length of 1.503 Å is larger than previously reported values of 1.486 and 1.461 Å.[15,19]

The C_3-C_4 bond partly explains the high energy of ^{3}**TS**. As the cyclization proceeds, the interaction between electrons on the arms of the molecule increases. Out-of-plane electrons interact stronger as the molecule becomes more planar and in-plane electrons interact stronger as the two arms are brought closer together. In-phase and out-of-phase orbitals that were nearly degenerate for ^{3}**R** are now energetically separated. ^{3}**TS** MOs that bring in-phase electron densities together, such as orbitals 9a, 8b, and 10b, are stabilized, while orbitals that bring out-of-phase densities together, such as orbitals 10a, 9b, and 11a, are destabilized (Figure 4). Altogether, there is a net destabilization, resulting in the high energy of ^{3}**TS**. This is also supported by analysis of natural orbitals in Figure 7.

In contrast to ^{1}**P**, the electronic structure of ^{3}**P** is dominated by a single configuration. The SOMOs of ^{3}**P** are the in-phase and out-of-phase combinations of the radical lobes on C_2 and C_5, with the out-of-phase combination being lower in energy.

Wave Function Properties and Natural Orbitals. Comparing energy-ordered MOs (Figure 5) with frontier orbitals obtained from population-ordered natural orbitals (Figures 6 and 7) shows good agreement with respect to both character and ordering. Average occupations, $\bar{n}$, show how many electrons are assigned to these orbitals. For the singlet product, $\bar{n}$ shows higher occupation of the natural orbitals arising from the in-phase radical bonding lobes and lower occupation of the NO corresponding to out-of-phase lobes (relative to ^{1}**TS**), consistent with increased diradical character. For the triplet wave functions (Figure 7), we see that both frontier natural orbitals are singly occupied at each stationary point on the reaction pathway.

Although the character of the MOs and NOs is consistent, the energy ordering of the MOs is not always indicative of the population ordering of the NOs. This is particularly true of doubly occupied orbitals, where one can see a reordering of natural orbitals that have nearly degenerate occupations.

Table 2 summarizes the wave function properties. $\langle S^2\rangle$ and parenthetical Δn values in Figures 6 and 7 indicate very little spin-contamination of the states. Parenthetical Δn values are high for frontier orbitals along the triplet pathway because these orbitals are associated with the $M_s = 1$ triplet and are therefore occupied by a single α electron. Along the singlet pathway, $n_{u,nl}$ indicates slight radical character even for ^{1}**R** and ^{1}**TS**, with a significant amount of radical character ($n_{u,nl} = 0.28$) observed for ^{1}**P**.

Energetics. Our activation energy ($\Delta H^{\ddagger}$) and energy of reaction (ΔH_{rxn}) of the cyclization reaction of ^{1}**R** are within 1 kcal/mol of Jones and Bergman's original findings of 32 and 14 kcal/mol, respectively (Figure 8).[1] In addition, although our $\Delta H^{\ddagger}$ is slightly greater than the value of 28.1 ± 1.6 kcal/mol reported by Wenthold and Squires, our ΔH_{rxn} agrees well with their value of 13 ± 3 kcal/mol.[61] Our cyclization energetics differ from those reported by Roth et al. (Table 3).[62]

To the best of our knowledge, no experimental results exist for the cyclization of ^{3}**R**, so we can only compare with other theoretical studies. For the triplet cyclization, our $\Delta H^{\ddagger}$ value is significantly higher and our ΔH_{rxn} is considerably less exothermic than previous results (Table 3).[15,19] Our characterization of ^{3}**TS** is fundamentally different, as evidenced by significant difference in the C_3-C_4 bond length, and produces a higher activation energy than the previous studies of Dong and Clark.[15,19] Alternatively, if our absolute energy for ^{3}**R** is much lower than absolute energies found by Dong and Clark, but the absolute energies of ^{3}**TS** and ^{3}**P** are similar, it would explain the relatively large activation barrier and less exothermic reaction enthalpy calculated in this study.

Table 4 lists vertical and adiabatic singlet−triplet gaps calculated for each structure. Our calculated singlet−triplet adiabatic gap value of 3.56 kcal/mol is in excellent agreement with Wenthold and Squire's experimental value of 3.8 ± 0.4 kcal/mol.[23]

Method Comparison. In this study, we explored multiple methods, basis sets, and reference wave functions. In Tables S3−S6, the energies are for the singlet reaction, which required a more complicated high-spin correction method (see Figure 2 for details of correction). The values in Tables S7−S10 are for the triplet reaction and are calculated by applying a ZPE correction to the raw energies of each triplet structure and then taking the difference, i.e., $H(\mathbf{P}) - H(\mathbf{R}) = \Delta H_{rxn}$.

For the singlet reaction, basis set effects are significant, i.e., increasing the basis set from cc-pVDZ to cc-pVTZ results in an approximately 3 and 5 kcal/mol difference in the $^1\Delta H^{\ddagger}$ and $^1\Delta H_{rxn}$, respectively. However, this effect is less pronounced in the triplet reaction. The differences in basis-set sensitivity between the singlet and triplet surfaces are expected; electron coupling and the multiconfigurational nature of the singlet increases the importance of dynamical correlation, which is better described with a larger basis set. It is also possible that the additional polarization functions in the triple-ζ basis allow for better characterization of the long-range interactions between the triple bond-containing arms of **R** and **TS** as well as the through bond coupling in **P**. The inclusion of triple excitations (CCSD vs CCSD(T)) produces a difference of ∼1 kcal/mol for the singlet surface. We do see a relatively large difference in the CCSD and CCSD(T) values of $^3\Delta H^{\ddagger}$ but not in the values for ΔH_{rxn}. This underscores the utility of using CCSD(T) results on the high-spin pathway in conjunction with SF singlet−triplet gaps to characterize the low-spin pathway. The inclusion of triple excitations (T) is important for quantitative accuracy and the balanced nature of the SF approach captures these effects accurately.

DOI: 10.1021/acs.jpca.7b10576
J. Phys. Chem. A 2018, 122, 420−430

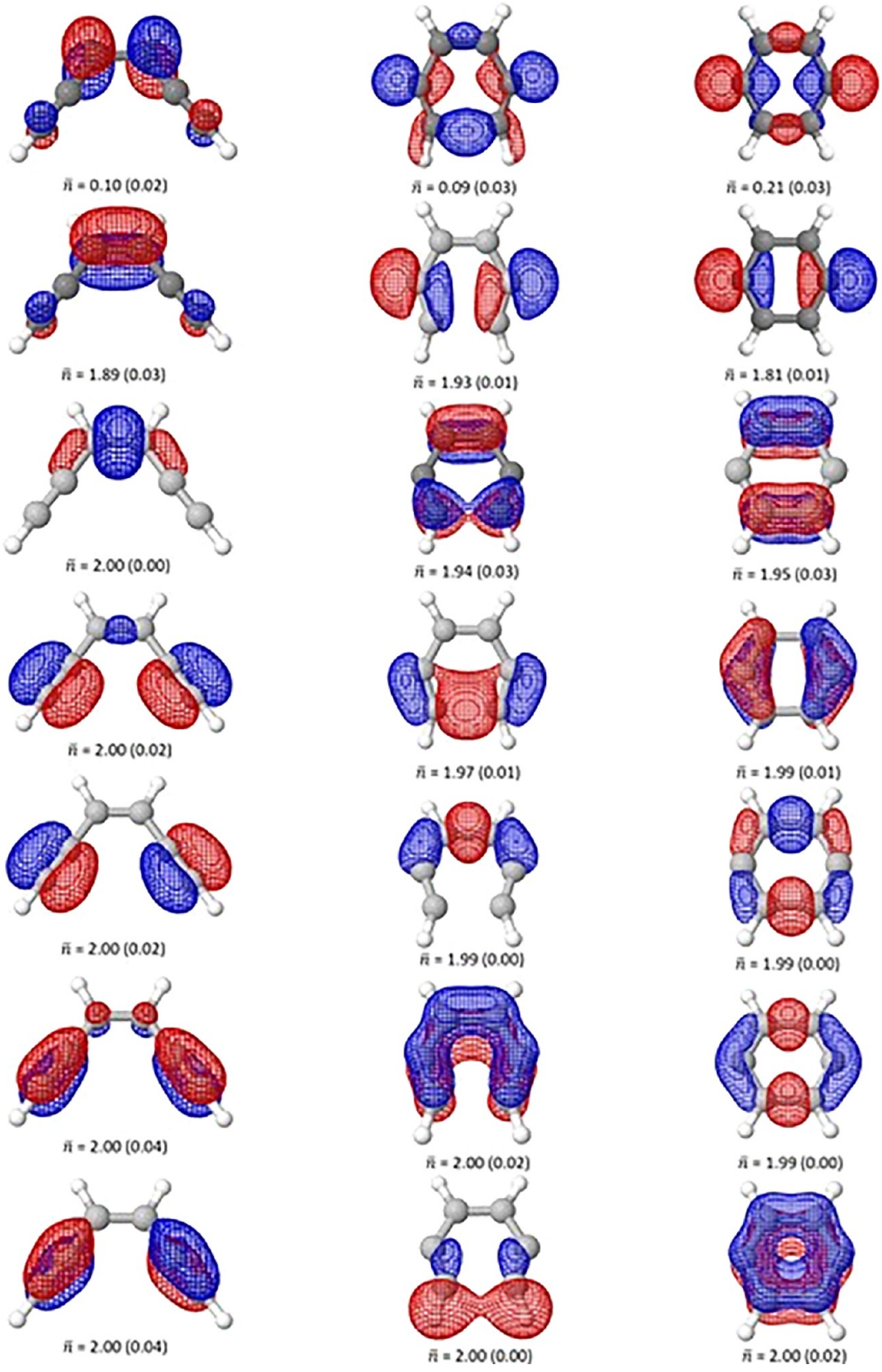

Figure 6. CCSD/cc-pVDZ frontier natural orbitals of the singlet states of the reactant (left), transition state (middle), and product (right) in the singlet pathway of Bergman cyclization. α-orbitals are shown. $\bar{n} = |n_\alpha + n_\beta|$, with $\Delta n = |n_\alpha - n_\beta|$ provided in parentheses.

CONCLUSIONS

The singlet and triplet pathways of the Bergman cyclization were characterized using reliable and robust coupled-cluster methods, CCSD, CCSD(T), and EOM-SF-CCSD. We found that the singlet pathway has a barrier of 32.75 kcal/mol and is endothermic by 13.76 kcal/mol. We determined that the triplet pathway has a barrier of 26.59 kcal/mol and is exothermic by 33.29 kcal/mol. We show that ^{1}**TS** is dominated by a single electronic configuration that is reactant-like in electronic structure but is geometrically very similar to ^{1}**P**. Both ^{3}**R** and ^{3}**TS** were found to have C_2 geometries. The analysis of frontier orbitals of each stationary point allowed us

DOI: 10.1021/acs.jpca.7b10576
J. Phys. Chem. A 2018, 122, 420−430

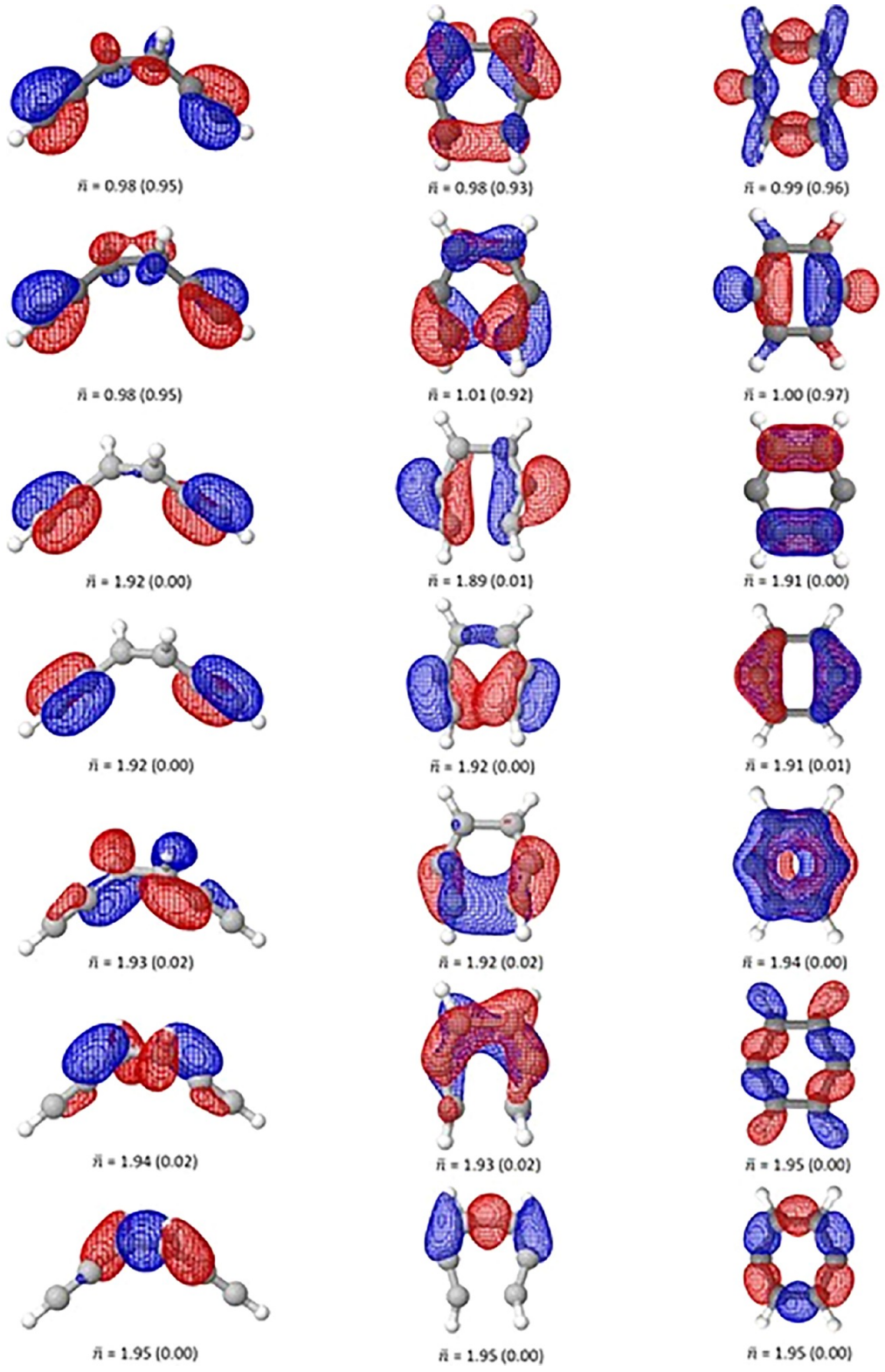

Figure 7. CCSD/cc-pVDZ frontier natural orbitals of high-spin triplet states of the reactant (left), transition state (middle), and product (right) in the triplet pathway of Bergman cyclization. α-orbitals are shown. $\overline{n} = |n_\alpha + n_\beta|$, with $\Delta\ n = |n_\alpha - n_\beta|$ provided in parentheses.

to explain the large energetic costs of the triplet cyclization; this high barrier is consistent with the findings of Turro and workers who concluded that the triplet pathway is not operational.[4]

This study illustrates the effectiveness of SF methods in characterizing reactions involving both closed- and open-shell species. Occupancy-ordered frontier natural orbitals generally agree with energy-ordered MOs. Density-based wave function analysis reveals the slight open-shell character of ^{1}**R** and ^{1}**TS** ($n_{u,nl}$ = 0.10 and 0.09 unpaired electrons, respectively) and the more pronounced radical character of ^{1}**P** ($n_{u,nl}$ = 0.28).

DOI: 10.1021/acs.jpca.7b10576
J. Phys. Chem. A 2018, 122, 420−430

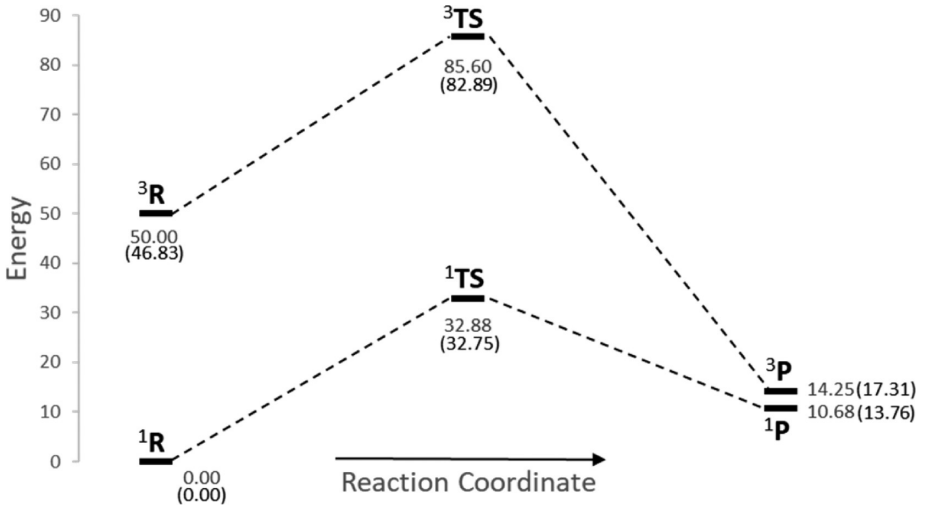

Figure 8. Energetic diagram along S_0 and T_1 pathways. Relative electronic energies are shown and ZPE-corrected energies are in parentheses. All values are in kcal/mol. The ^{3}**R** energy shown is the **R** adiabatic ΔE_{ST}. The ^{3}**TS** and ^{3}**P** energies relative to ^{1}**R** were calculated by adding the **TS** and **P** adiabatic $\Delta E_{ST,a}$ to the to the energy of ^{1}**TS** and ^{1}**P**, respectively.

Table 3. $\Delta H^{\ddagger}$ and ΔH_{rxn} Values for S_0 and T_1 Cyclizations Alongside Available Experimental and Previous Theoretical Values

	$^1\Delta H^{\ddagger}$	$^1\Delta H_{rxn}$	$^3\Delta H^{\ddagger}$	$^3\Delta H_{rxn}$
expt	32,[a] 28.2,[b] 28.1 ± 1.6[c]	14,[a] 8.5,[b] 13 ± 3[c]		
this work	32.75	13.76	26.59[d]	−33.29[d]
CCSD(T)/6-31G(d,p)	28.5	8		
CASMP2/6-31G*	24.22	−4.92	21.42	−41.8
CASPT2(12,12)/ANO-L	25.6	12.2	22.2	−37
B3LYP/6-31G**	31.2	3.3	23.7	−45.2

[a]Reference 1. [b]Reference 62. [c]Reference 61. [d]These values are computed directly between triplet structure total energies. They do not match the ones reported in the figure above, which were calculated relative to ^{1}R.

Table 4. Vertical Singlet−Triplet Gaps for Each Structure[a]

structure	vertical ΔE_{ST}	adiabatic ΔE_{ST}
^{1}**R**	130.9	46.83
^{3}**R**	1.11	
^{1}**TS**	42.78	50.14
^{3}**TS**	22.32	
^{1}**P**	5.14	3.56
^{3}**P**	3.15	

[a]Adiabatic gaps for **R**, **TS**, and **P** (ZPE-corrected). All values are in kcal/mol. A positive value indicates that the singlet is lower in energy.

■ ASSOCIATED CONTENT

Supporting Information

The Supporting Information is available free of charge on the ACS Publications website at DOI: 10.1021/acs.jpca.7b10576.

Absolute and relative energies calculated with a variety of methodological treatments, a comparison of energies obtained with a restricted and unrestricted reference, zero-point energies, molecular orbital energies, a comparison of singlet and triplet TS geometries computed with different treatments, and Cartesian coordinates for all species (PDF)

■ AUTHOR INFORMATION

Corresponding Author

*C. A. Parish. E-mail: cparish@richmond.edu.

ORCID

Anna I. Krylov: 0000-0001-6788-5016

Carol A. Parish: 0000-0003-2878-3070

Notes

The authors declare no competing financial interest.

■ ACKNOWLEDGMENTS

C.A.P. acknowledges support from the Department of Energy (Grant DE-SC0001093), NSF RUI (Grant CHE-1213271) and the Donors of the American Chemical Society Petroleum Research Fund. A.R.L. acknowledges support from the Arnold and Mabel Beckman Foundation through receipt of a Beckman Scholars award. A.K. acknowledges support by the U.S. Air Force of Scientific Research (AFOSR) under contractor number FA9550-16-1-0051.

■ REFERENCES

(1) Jones, R. R.; Bergman, R. G. P-Benzyne. Generation as an Intermediate in a Thermal Isomerization Reaction and Trapping Evidence for the 1, 4-Benzenediyl Structure. *J. Am. Chem. Soc.* **1972**, *94*, 660−661.

(2) Nath, M.; Pink, M.; Zaleski, J. M. Controlling Both Ground-and Excited-State Thermal Barriers to Bergman Cyclization with Alkyne Termini Substitution. *J. Am. Chem. Soc.* **2005**, *127*, 478−479.

(3) Cambell, I. D.; Eglinton, G. A Novel Photochemical Cyclisation of O-Bisiodoethynylbenzene to Substituted Naphthalenes. *J. Chem. Soc. C* **1968**, 2120−2121.

(4) Turro, N. J.; Evenzahav, A.; Nicolaou, K. C. Photochemical Analogue of the Bergman Cycloaromatization Reaction. *Tetrahedron Lett.* **1994**, *35*, 8089−8092.

(5) Evenzahav, A.; Turro, N. J. Photochemical Rearrangement of Enediynes: Is a "Photo-Bergman" Cyclization a Possibility? *J. Am. Chem. Soc.* **1998**, *120*, 1835−1841.

(6) Papp, P.; Neogrady, P.; Mach, P.; Pittner, J.; Huba, I.; Wilson, S. Many-Body Brillouin−Wigner Second-Order Perturbation Theory: An Application to the Autoaromatisation of Hex-3-Ene-1,5-Diyne (the Bergman Reaction). *Mol. Phys.* **2008**, *106*, 57−74.

(7) Kagan, J.; Wang, X.; Chen, X.; Lau, K. Y.; Batac, I. V.; Tuveson, R. W.; Hudson, J. B. DNA Cleavage, Antiviral and Cytotoxic

DOI: 10.1021/acs.jpca.7b10576
J. Phys. Chem. A 2018, 122, 420−430

Reactions Photosensitized by Simple Enediyne Compounds. *J. Photochem. Photobiol., B* **1993**, *21*, 135−142.
(8) Halter, R. J.; Fimmen, R. L.; McMahon, R. J.; Peebles, S. A.; Kuczkowski, R. L.; Stanton, J. F. Microwave Spectra and Molecular Structures of (Z)-Pent-2-En-4-Ynenitrile and Maleonitrile. *J. Am. Chem. Soc.* **2001**, *123*, 12353−12363.
(9) Nicolaou, K.; Liu, A.; Zeng, Z.; McComb, S. Redox-Controlled Bergman Cycloaromatizations. Designed Enediynes with DNA-Cleaving Properties and Antitumor Activity. *J. Am. Chem. Soc.* **1992**, *114*, 9279−9282.
(10) Nicolaou, K. C.; Smith, A. L. Molecular Design, Chemical Synthesis, and Biological Action of Enediynes. *Acc. Chem. Res.* **1992**, *25*, 497−503.
(11) Nicolaou, K. C.; Smith, A. L.; Yue, E. W. Chemistry and Biology of Natural and Designed Enediynes. *Proc. Natl. Acad. Sci. U. S. A.* **1993**, *90*, 5881−5888.
(12) Cramer, C. J. Bergman, Aza-Bergman, and Protonated Aza-Bergman Cyclizations and Intermediate 2,5-Arynes: Chemistry and Challenges to Computation. *J. Am. Chem. Soc.* **1998**, *120*, 6261−6269.
(13) Gräfenstein, J.; Hjerpe, A. M.; Kraka, E.; Cremer, D. An Accurate Description of the Bergman Reaction Using Restricted and Unrestricted Dft: Stability Test, Spin Density, and on-Top Pair Density. *J. Phys. Chem. A* **2000**, *104*, 1748−1761.
(14) Alabugin, I. V.; Manoharan, M. Radical-Anionic Cyclizations of Enediynes: Remarkable Effects of Benzannelation and Remote Substituents on Cyclorearomatization Reactions. *J. Am. Chem. Soc.* **2003**, *125*, 4495−4509.
(15) Dong, H.; Chen, B. Z.; Huang, M. B.; Lindh, R. The Bergman Cyclizations of the Enediyne and Its N-Substituted Analogs Using Multiconfigurational Second-Order Perturbation Theory. *J. Comput. Chem.* **2012**, *33*, 537−49.
(16) Kraka, E.; Cremer, D. Ccsd (T) Investigation of the Bergman Cyclization of Enediyne. Relative Stability of O-, M-, and P-Didehydrobenzene. *J. Am. Chem. Soc.* **1994**, *116*, 4929−4936.
(17) Schreiner, P. R.; Navarro-Vázquez, A.; Prall, M. Computational Studies on the Cyclizations of Enediynes, Enyne-Allenes, and Related Polyunsaturated Systems. *Acc. Chem. Res.* **2005**, *38*, 29−37.
(18) Koga, N.; Morokuma, K. Comparison of Biradical Formation between Enediyne and Enyne-Allene. Ab Initio Casscf and Mrsdci Study. *J. Am. Chem. Soc.* **1991**, *113*, 1907−1911.
(19) Clark, A. E.; Davidson, E. R.; Zaleski, J. M. Udft and Mcscf Descriptions of the Photochemical Bergman Cyclization of Enediynes. *J. Am. Chem. Soc.* **2001**, *123*, 2650−2657.
(20) Lindh, R.; Lee, T. J.; Bernhardsson, A.; Persson, B. J.; Karlstroem, G. Extended Ab Initio and Theoretical Thermodynamics Studies of the Bergman Reaction and the Energy Splitting of the Singlet O-, M-, and P-Benzynes. *J. Am. Chem. Soc.* **1995**, *117*, 7186−7194.
(21) Galbraith, J. M.; Schreiner, P. R.; Harris, N.; Wei, W.; Wittkopp, A.; Shaik, S. A Valence Bond Study of the Bergman Cyclization: Geometric Features, Resonance Energy, and Nucleus-Independent Chemical Shift (Nics) Values. *Chem. - Eur. J.* **2000**, *6*, 1446−1454.
(22) McMahon, R. J.; Halter, R. J.; Fimmen, R. L.; Wilson, R. J.; Peebles, S. A.; Kuczkowski, R. L.; Stanton, J. F. Equilibrium Structure of Cis-Hex-3-Ene-1,5-Diyne and Relevance to the Bergman Cyclization. *J. Am. Chem. Soc.* **2000**, *122*, 939−949.
(23) Wenthold, P. G.; Squires, R. R.; Lineberger, W. C. Ultraviolet Photoelectron Spectroscopy of the O-, M-, and P-Benzyne Negative Ions. Electron Affinities and Singlet−Triplet Splittings for O-, M-, and P-Benzyne. *J. Am. Chem. Soc.* **1998**, *120*, 5279−5290.
(24) Wang, E. B.; Parish, C. A.; Lischka, H. An Extended Multireference Study of the Electronic States of Para-Benzyne. *J. Chem. Phys.* **2008**, *129*, 044306.
(25) Bernard, Y. A.; Shao, Y.; Krylov, A. I. General Formulation of Spin-Flip Time-Dependent Density Functional Theory Using Non-Collinear Kernels: Theory, Implementation, and Benchmarks. *J. Chem. Phys.* **2012**, *136*, 204103.
(26) Yang, Y.; Peng, D.; Davidson, E. R.; Yang, W. Singlet−Triplet Energy Gaps for Diradicals from Particle−Particle Random Phase Approximation. *J. Phys. Chem. A* **2015**, *119*, 4923−4932.
(27) Slipchenko, L. V.; Krylov, A. I. Singlet-Triplet Gaps in Diradicals by the Spin-Flip Approach: A Benchmark Study. *J. Chem. Phys.* **2002**, *117*, 4694−4708.
(28) Salem, L.; Rowland, C. The Electronic Properties of Diradicals. *Angew. Chem., Int. Ed. Engl.* **1972**, *11*, 92−111.
(29) Crawford, T. D.; Kraka, E.; Stanton, J. F.; Cremer, D. Problematic P-Benzyne: Orbital Instabilities, Biradical Character, and Broken Symmetry. *J. Chem. Phys.* **2001**, *114*, 10638−10650.
(30) Greenman, L.; Mazziotti, D. A. Highly Multireferenced Arynes Studied with Large Active Spaces Using Two-Electron Reduced Density Matrices. *J. Chem. Phys.* **2009**, *130*, 184101.
(31) Clark, T. Reviews in Computational Chemistry Iv. Edited by K. B. Lipkowitz and D. B. Boyd, Vch Weinheim 1993, Xix, 280 Pp., Hardcover, Dm 138, Isbn 3−527−89520−1. *Adv. Mater.* **1994**, *6*, 88−88.
(32) Krylov, A. I. Spin-Flip Configuration Interaction: An Electronic Structure Model That Is Both Variational and Size-Consistent. *Chem. Phys. Lett.* **2001**, *350*, 522−530.
(33) Krylov, A. I. Spin-Flip Equation-of-Motion Coupled-Cluster Electronic Structure Method for a Description of Excited States, Bond Breaking, Diradicals, and Triradicals. *Acc. Chem. Res.* **2006**, *39*, 83−91.
(34) Slipchenko, L. V.; Krylov, A. I. Spin-Conserving and Spin-Flipping Equation-of-Motion Coupled-Cluster Method with Triple Excitations. *J. Chem. Phys.* **2005**, *123*, 084107.
(35) Krylov, A. I. Equation-of-Motion Coupled-Cluster Methods for Open-Shell and Electronically Excited Species: The Hitchhiker's Guide to Fock Space. *Annu. Rev. Phys. Chem.* **2008**, *59*, 433−462.
(36) Golubeva, A. A.; Nemukhin, A. V.; Klippenstein, S. J.; Harding, L. B.; Krylov, A. I. Performance of the Spin-Flip and Multireference Methods for Bond Breaking in Hydrocarbons: A Benchmark Study. *J. Phys. Chem. A* **2007**, *111*, 13264−13271.
(37) Hossain, E.; Deng, S. M.; Gozem, S.; Krylov, A. I.; Wang, X.-B.; Wenthold, P. G. Photoelectron Spectroscopy Study of Quinonimides. *J. Am. Chem. Soc.* **2017**, *139*, 11138−11148.
(38) Vanovschi, V.; Krylov, A. I.; Wenthold, P. G. Structure, Vibrational Frequencies, Ionization Energies, and Photoelectron Spectrum of the Para-Benzyne Radical Anion. *Theor. Chem. Acc.* **2008**, *120*, 45−58.
(39) Manohar, P. U.; Krylov, A. I. A Noniterative Perturbative Triples Correction for the Spin-Flipping and Spin-Conserving Equation-of-Motion Coupled-Cluster Methods with Single and Double Substitutions. *J. Chem. Phys.* **2008**, *129*, 194105.
(40) Levchenko, S. V.; Krylov, A. I. Equation-of-Motion Spin-Flip Coupled-Cluster Model with Single and Double Substitutions: Theory and Application to Cyclobutadiene. *J. Chem. Phys.* **2004**, *120*, 175−185.
(41) Stanton, J. F.; Bartlett, R. J. The Equation of Motion Coupled-Cluster Method. A Systematic Biorthogonal Approach to Molecular Excitation Energies, Transition Probabilities, and Excited State Properties. *J. Chem. Phys.* **1993**, *98*, 7029−7039.
(42) Purvis, G. D., III; Bartlett, R. J. A Full Coupled-Cluster Singles and Doubles Model: The Inclusion of Disconnected Triples. *J. Chem. Phys.* **1982**, *76*, 1910−1918.
(43) Plasser, F.; Bäppler, S. A.; Wormit, M.; Dreuw, A. New Tools for the Systematic Analysis and Visualization of Electronic Excitations. *J. Chem. Phys.* **2014**, *141*, 024107.
(44) Plasser, F.; Wormit, M.; Dreuw, A. New Tools for the Systematic Analysis and Visualization of Electronic Excitations. I. Formalism. *J. Chem. Phys.* **2014**, *141*, 024106.
(45) Orms, N.; Rehn, D.; Dreuw, A.; Krylov, A. I. Characterizing Bonding Patterns in Diradicals and Triradicals by Density-Based Wave Function Analysis: A Uniform Approach. *J. Chem. Theory Comput.* **2017**, DOI: 10.1021/acs.jctc.7b01012.
(46) Takatsuka, K.; Fueno, T.; Yamaguchi, K. Distribution of Odd Electrons in Ground-State Molecules. *Theor. Chim. Acta* **1978**, *48*, 175−183.

DOI: 10.1021/acs.jpca.7b10576
J. Phys. Chem. A 2018, 122, 420−430

(47) Head-Gordon, M. Characterizing Unpaired Electrons from the One-Particle Density Matrix. *Chem. Phys. Lett.* **2003**, *372*, 508−511.
(48) Luzanov, A. V. Effectively Unpaired Electrons for Singlet States: From Diatomics to Graphene Nanoclusters. In *Practical Aspects of Computational Chemistry IV*; Leszczynski, J., Shukla, M. K., Eds.; Springer-Verlag: New York, 2016; pp 151−206.
(49) Shao, Y.; Gan, Z.; Epifanovsky, E.; Gilbert, A. T. B.; Wormit, M.; Kussmann, J.; Lange, A. W.; Behn, A.; Deng, J.; Feng, X.; et al. Advances in Molecular Quantum Chemistry Contained in the Q-Chem 4 Program Package. *Mol. Phys.* **2015**, *113*, 184−215.
(50) Anet, F. A. L.; Rawdah, T. N. Iterative Force-Field Calculations of Cycloudecane, Cyclotridecane, and Cyclopentadecane. *J. Am. Chem. Soc.* **1978**, *100*, 7810−7814.
(51) Kemp, D. S. Intramolecular O,N-Acyl Transfer Via Cyclic Intermediates of Nine and Twelve Members. Models for Extensiona of the Amine Capture Strategy for Peptide Sythesis. *J. Am. Chem. Soc.* **1981**, *46*, 490−498.
(52) Cristian, A.-M. C.; Shao, Y.; Krylov, A. I. Bonding Patterns in Benzene Triradicals from Structural, Spectroscopic, and Thermochemical Perspectives. *J. Phys. Chem. A* **2004**, *108*, 6581−6588.
(53) Hehre, W. J.; Ditchfield, R.; Radom, L.; Pople, J. A. Molecular Orbital Theory of the Electronic Structure of Organic Compounds. V. Molecular Theory of Bond Separation. *J. Am. Chem. Soc.* **1970**, *92*, 4796−4801.
(54) Pople, J. A.; Radom, L.; Hehre, W. J. Molecular Orbital Theory of the Electronic Structure of Organic Compounds. Vii. Systematic Study of Energies, Conformations, and Bond Interactions. *J. Am. Chem. Soc.* **1971**, *93*, 289−300.
(55) Hehre, W. J.; Radom, L.; Schleyer, P. v. R.; Pople, J. A. *Ab Initio Molecular Orbital Theory*; Wiley-Interscience: New York, 1986.
(56) Wheeler, S. E.; Houk, K. N.; Schleyer, P. v. R.; Allen, W. D. A Hierarchy of Homodesmotic Reactions for Thermochemistry. *J. Am. Chem. Soc.* **2009**, *131*, 2547−2560.
(57) Cramer, C. J.; Nash, J. J.; Squires, R. R. A Reinvestigation of Singlet Benzyne Thermochemistry Predicted by Caspt2, Coupled-Cluster and Density Functional Calculations. *Chem. Phys. Lett.* **1997**, *277*, 311−320.
(58) Krylov, A. I. The Quantum Chemistry of Open-Shell Species. In *Reviews in Computational Chemistry Vol. 30*, Parrill, A. L., Lipkowitz, K. B., Eds.; Wiley: Hoboken, NJ, 2017; pp 151−224.
(59) Hoffmann, R. Interaction of Orbitals through Space and through Bonds. *Acc. Chem. Res.* **1971**, *4*, 1−9.
(60) Hoffmann, R.; Imamura, A.; Hehre, W. J. Benzynes, Dehydroconjugated Molecules, and the Interaction of Orbitals Separated by a Number of Intervening Sigma Bonds. *J. Am. Chem. Soc.* **1968**, *90*, 1499−1509.
(61) Wenthold, P. G.; Squires, R. R. Biradical Thermochemistry from Collision-Induced Dissociation Threshold Energy Measurements. Absolute Heats of Formation of Ortho-, Meta-, and Para-Benzyne. *J. Am. Chem. Soc.* **1994**, *116*, 6401−6412.
(62) Roth, W. R.; Hopf, H.; Horn, C. 1,3,5-Cyclohexatrien-1,4-Diyl Und 2,4-Cyclohexadien-1,4-Diyl. *Chem. Ber.* **1994**, *127*, 1765−1779.

DOI: 10.1021/acs.jpca.7b10576
J. Phys. Chem. A 2018, 122, 420−430